New Constraints on the Existence of Massive Monopoles in Ultra-Peripheral Heavy Ion Collisions with ATLAS

K. Cieśla,[a] on behalf of the ATLAS Collaboration
AGH University of Kraków, al. Adama Mickiewicza 30, Kraków, 30-059, Poland

In ultraperipheral Pb+Pb collisions, intense electromagnetic fields enable the generation of magnetic monopole pairs via the Schwinger mechanism. Due to their high ionization and unique trajectories in a solenoidal magnetic field, monopoles are expected to leave numerous clusters in the innermost ATLAS pixel detector without associated reconstructed charged-particle tracks or calorimeter activity. This document presents a search for monopole-pair production in ultraperipheral Pb+Pb collisions with a magnetic charge of $q_m = 1g_D$ in the monopole mass range of 20–150 GeV, based on 5.36 TeV data recorded in 2023. The results are compared with a recently developed semiclassical model that includes non-perturbative cross-section calculations – as well as with a recent search limits obtained by the MoEDAL Collaboration using complementary techniques.

DOI: https://doi.org/10.17161/ncjh2x81
Keywords: ultraperipheral collisions, magnetic monopoles production

1 Introduction

1.1 Ultra-Peripheral heavy-ion collisions

The relativistic heavy-ion collisions at the Large Hadron Collider [1] (LHC) provide a wide range of unique measurement opportunities. A significant part of the LHC heavy-ion programme consists of measuring ultraperipheral collisions (UPC) where ions do not collide directly, but instead interact via their electromagnetic fields. Colliding ions are an intense source of quasi-real photons, with each photon flux scaling with the square of the charge of the nucleus. The UPC events can be used to study many photon-induced processes such as exclusive dilepton production ($\gamma\gamma \to l^+l^-$) [2,3,4] or light-by-light scattering ($\gamma\gamma \to \gamma\gamma$) [5], as well as beyond the Standard Model searches, e.g. τ-lepton anomalous magnetic moment [4], axion-like particles [5] or, in particular, magnetic monopole ($M\bar{M}$) production [6].

1.2 Magnetic monopoles

Magnetic monopoles are hypothetical particles that carry isolated magnetic charge. The existence of such particles would not only restore symmetry to Maxwell's equations, but also explain why electric charge is quantized in nature, as it was proposed by Dirac [7]. Dirac postulated that a magnetic charge of a magnetic monopole would be equal to $q_m = ng_D$, where n is an integer number, and $g_D = e/2\alpha = 68.5e$ is the Dirac elementary charge.[b] With a such property, the magnetic monopoles would manifest as a highly ionising particle.

In UPC collisions, the primary mechanism via which magnetic monopoles could be produced is the Schwinger mechanism [8]. In this formalism, the electrically charged particles could be produced in a strong electric field by tunnelling through the Coulomb barrier. If magnetic monopoles exist, electromagnetic duality implies that $M\bar{M}$ would also be produced by the same mechanism, in a sufficiently strong magnetic field. Such process is schematically shown in Figure 1. With this mechanism, the $M\bar{M}$ production cross-section can be calculated non-perturbatively using semiclassical techniques, such as free-particle approximation (FPA) [9] or locally constant field approximation (LCFA) [9,10,11,12] models.

The first search for $M\bar{M}$ production in Pb+Pb collisions was performed by the MoEDAL experiment based on the 5.02 TeV heavy-ion run at the LHC in November 2018 [11]. MoEDAL trapping detectors were exposed to 235 µb^{-1} of Pb+Pb collisions, which allowed the exclusion of production of monopoles in UPC with Dirac charges between $1gD$ and $3gD$ and masses up to 75 GeV. Another MoEDAL search using the CMS beampipe [12] allowed the exclusion of the same process in the very broad charge range, between $2gD$ and $45gD$. The search presented here [6] uses 262 µb^{-1} of 5.36 TeV of Pb+Pb collision data

[a] Speaker, email: krzysztof.marcin.ciesla@cern.ch
[b] e – elementary electric charge, α – fine structure constant.

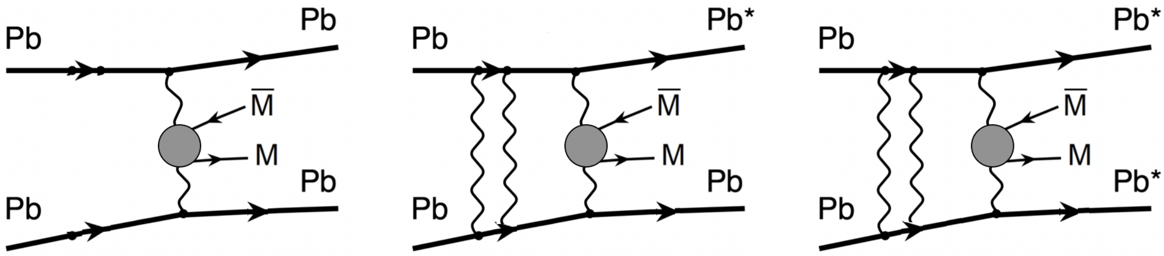

Figure 1 – Schematic diagrams for magnetic monopole pair production in ultraperipheral Pb+Pb collisions for (left) no, (middle) single and (right) mutual ion excitation due to extra soft-photon exchanges. Electromagnetic breakup of the ion, denoted by Pb*, results in the production of forward neutrons, detectable in the ATLAS ZDC.

collected in 2023 by the ATLAS experiment. The magnetic monopoles considered in this search have magnetic charge equal to one Dirac charge and masses between 20 GeV and 150 GeV.

2 ATLAS experiment

The ATLAS experiment [13,14] at the LHC is a multipurpose particle detector with a forward–backward symmetric cylindrical geometry and a near 4π coverage in solid angle.[c] It consists of an inner tracking detector surrounded by a thin superconducting solenoid providing a 2 T axial magnetic field, electromagnetic and hadronic calorimeters, and a muon spectrometer.

The inner-detector system (ID) is immersed in a 2 T axial magnetic field and provides charged-particle tracking in the range $|\eta| < 2.5$. The high-granularity silicon pixel detector covers the vertex region and typically provides four measurements per track, the first hit generally being in the insertable B-layer (IBL). It is followed by the SemiConductor Tracker (SCT), which usually provides eight measurements per track. These silicon detectors are complemented by the transition radiation tracker (TRT), which enables radially extended track reconstruction up to $|\eta| = 2.0$. The TRT also provides electron identification information based on the fraction of hits (typically 30 in total) above a higher energy-deposit threshold corresponding to transition radiation.

Lead/liquid-argon (LAr) sampling calorimeters provide electromagnetic (EM) energy measurements with high granularity within the region $|\eta| < 3.2$. A steel/scintillator-tile hadronic calorimeter covers the central pseudorapidity range ($|\eta| < 1.7$). The endcap and forward regions are instrumented with LAr calorimeters for EM and hadronic energy measurements up to $|\eta| = 4.9$.

The muon spectrometer surrounds the calorimeters and is based on three large superconducting air-core toroidal magnets with eight coils each. The field integral of the toroids ranges between 2.0 and 6.0 Tm across most of the detector. The muon spectrometer includes a system of precision tracking chambers up to $|\eta| = 2.7$ and fast detectors for triggering up to $|\eta| = 2.4$. The luminosity is measured mainly by the LUCID–2 detector which is located close to the beampipe.

A two-level trigger system was used to select events [15]. The first-level trigger is implemented in hardware and used a subset of the detector information to accept events at a rate close to 100 kHz. This is followed by a software-based trigger that reduced the accepted rate of complete events to 3 kHz on average, depending on the data-taking conditions. A software suite [16] is used in Monte Carlo (MC) simulation, in the reconstruction and analysis of real and simulated data, in detector operations, and in the trigger and data acquisition systems of the experiment.

The zero-degree calorimeter (ZDC) consists of four longitudinal compartments on each side of the interaction point (IP), each with one nuclear interaction length of tungsten absorber plates interleaved with a row of 1.5 mm-diameter quartz rods. Light produced by Cherenkov radiation from shower products is transported up to the top of the detector, guided through a trapezoidal prism light guide and into a photomultiplier tube assembly. The detectors are located 140 m from the nominal IP in both directions,

[c] ATLAS uses a right-handed coordinate system with its origin at the nominal interaction point (IP) in the centre of the detector and the z-axis along the beam pipe. The x-axis points from the IP to the centre of the LHC ring, and the y-axis points upwards. Polar coordinates (r, ϕ) are used in the transverse plane, ϕ being the azimuthal angle around the z-axis. The pseudorapidity is defined in terms of the polar angle θ as $\eta = -\ln\tan(\theta/2)$ and is equal to the rapidity $y = \frac{1}{2}\ln\left(\frac{E+p_z}{E-p_z}\right)$ in the relativistic limit. Angular distance is measured in units of $\Delta R \equiv \sqrt{(\Delta y)^2 + (\Delta\phi)^2}$.

covering $|\eta| > 8.3$. They detect neutral particles such as neutrons emitted from interacting nuclei. The ZDC thresholds were set to select events with even a single neutron reaching the ZDC.

2.1 Interaction of magnetic monopoles with the detector

The energy loss of a charged particle interacting with the detector material is proportional the square of the particle's charge. Due to the highly-ionising nature of the magnetic monopoles, their interaction with the detector results in many times larger energy deposit compared to the minimally ionising particles. As an example, a magnetic monopole with magnetic charge of $q_m = 1g_D$ would result in energy deposit 4700 times larger compared to that of a proton.

The magnetic monopoles considered in this search have relatively low masses, below 150 GeV, and have often low energy. Let us consider production of magnetic monopoles pair, with monopoles with a mass of 20 GeV, transverse momentum p_T of 50 GeV, and "back-to-back" event topology and their subsequent interaction with the Inner Detector material. Figure 2 shows an event display of such simulated process.

When a such highly-ionising particle passes though the detector material, it kicks out numerous δ-electrons, which in turn are detected as an ordinary hits, forming the signal. Another unique experimental signature of the magnetic monopoles that can be exploited, is their behaviour in the solenoidal magnetic field. Compared to the electrically charged particles (bending in the transverse plane and no bending in the longitudinal plane), the magnetically charged particles will be accelerating in the solenoidal magnetic field, resulting in no bending in the transverse plane and a parabolic trajectory in the longitudinal plane. This leads to events with multiple Silicon clusters and no reconstructed charged-particle tracks.

Exploiting these unique experimental signatures is only possible in the extremely low pile-up [d] environment provided by the ultra-relativistic heavy-ion collisions.

3 Analysis strategy

3.1 Event selection

The search presented uses 262 µb^{-1} of 5.36 TeV of Pb+Pb collision data collected in 2023 by the ATLAS experiment. Monte Carlo (MC) simulated signal samples were produced using a semiclassical approach based on the FPA model. This semiclassical approximation breaks down for sufficiently light monopoles, m ¡ 20 GeV for 5.36 TeV Pb+Pb collisions, so monopole mass hypotheses below 20 GeV are not considered.

The events of interest are selected by the first-level trigger system, requiring the total energy deposited in the calorimeter to be less than 10 GeV and the $XnXn$ event topology, which denotes the presence of neutrons on both ZDC sides. In addition, at the high-level trigger, a presence of at least 100 pixel clusters is required.

To suppress collision background, the signal events are required to have at most one reconstructed charged-particle track (with transverse momentum p_T ¿ 0.1 GeV, $|\eta|$ ¡ 2.5, and a transverse impact

[d] Number of simultaneous collisions.

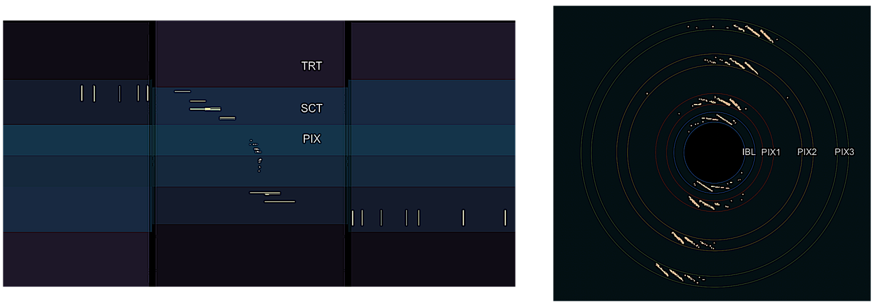

Figure 2 – Event display of simulated monopole pair production with detector conditions similar to that expected for Pb+Pb UPC for monopole mass of 20 GeV and transverse momentum $p_T = 50$ GeV. Shown are the longitudinal view of the full inner detector (left) and the transverse view of the Pixel detector (right), with the different layers denoted as IBL, PIX1, PIX2, and PIX3. Pixel hits are shown in light orange and SCT hits are denoted as yellow strips. The event topology is always "back-to-back" (due to momentum conservation) and so both monopoles have similar transverse momentum values.

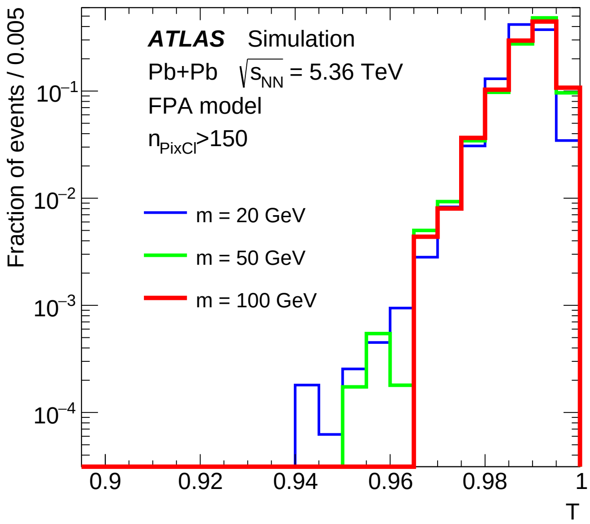

Figure 3 – Distribution of the T observable in simulated signal events passing all SR requirements, except for the T ¿ 0.95 requirement, for various monopole mass hypotheses.

parameter of $|d_0|$ ¡ 1 mm), and at most one topological cluster of calorimeter-cell energy deposits (with transverse energy E_T ¿ 0.1 GeV and $|\eta|$ ¡ 4.9). Events are also required to have at least 150 pixel clusters n_{PixCl} ¿ 150, with at least 50 of them originating from the innermost pixel layer. To suppress noisy Pixel detector modules, an additional requirement on the fraction of Pixel clusters originating from a single module $f_{leading-module}$ is set. Events with $f_{leading-module}$ ¿ 0.9 are rejected.

The background considered in the search is dominated by beam-induced background (BIB), caused by beam particle losses in the LHC ring upstream of the ATLAS experiment. It is characterized by particles almost parallel to the beam line, especially those with small radius [17]. To reduce its contribution a T variable, related to transverse thrust [18], is used:

$$T = \frac{1}{n_{PixCl}} \sum_{i=1}^{n_{PixCl}} |\hat{r_i} \cdot \hat{n}|, \tag{1}$$

where $\hat{r_i}$ is a direction of given pixel cluster in the transverse plane with respect to the origin of the ATLAS coordinate system, and $\hat{n}$ is the direction which maximizes the T value. Figure 3 shows the distribution of the T variable in the simulated signal events for several mass hypotheses. For the background events the T variable value is just above $2/\pi$ (not shown), while for the simulated signal it is close to unity. Therefore, a requirement of T ¿ 0.95 to define the signal region (SR) is used.

3.2 Background estimation

The beam-induced background is estimated using a fully data-driven method. The first control region (CR1) is defined by requiring $T \leq 0.87$, and it is observed that the characteristics of these events agree with those of BIB events. Due to the asymmetric nature of BIB events, a second control region (CR2) is defined from events having a $Xn0n$ topology – presence of neutrons only on one ZDC side. The same selection criteria as to the signal events were applied to the events in CR2, except for the T requirement, and a different topological cluster selection: between one and three topological clusters, with at least one of them being out-of-time (reconstructed time more than 10 ns before the bunch-crossing time). This allows to enrich the CR2 sample with BIB events and consequently reduce its signal contamination. Events in CR2 are used to extrapolate the background contribution from CR1 to SR by fitting:

$$N^{SR}_{bkg} = \frac{N^{CR1}}{N^{CR2}_{T<0.87}} N^{CR2}_{T>0.95}. \tag{2}$$

To cross-check this procedure, a validation region (VR) is defined by requiring 0.87 ¡ $T \leq 0.95$. Figure 4 (left) shows ϕ_T (direction of maximum T) distribution for data in the VR. The CR2-based background estimate describes the data well, and the enhanced activity at $\phi_T \approx 0$ and $\phi_T \approx \pi$ are characteristic of BIB [17].

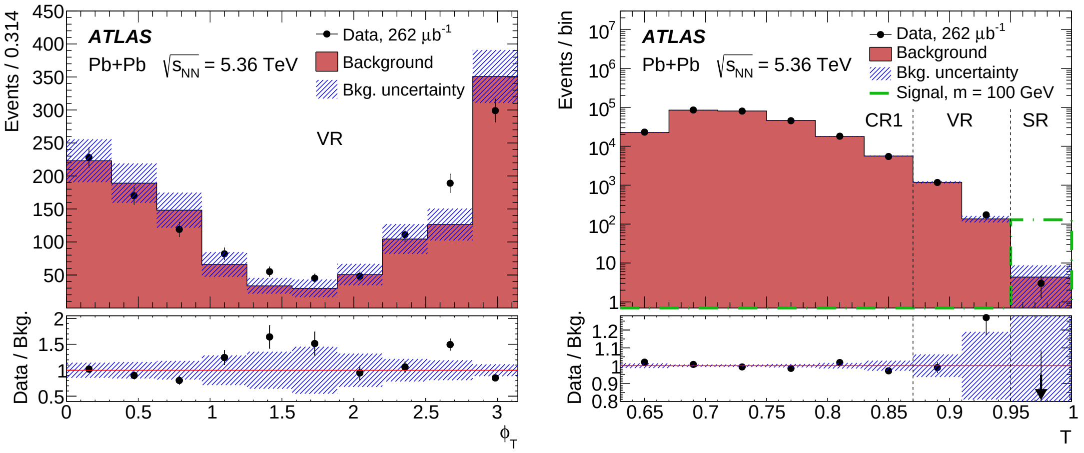

Figure 4 – ϕ_T distribution for data in the VR (left) and T distribution for data in CR1, the VR, and the SR (right). Data (markers) are shown together with the estimated background (filled histograms). The distributions for background use events from CR2 scaled as described in the text. The lower panels shows the ratio of data to the estimated background. The shaded bands represent the statistical uncertainty of the background. In right plot the green dotted-dashed line shows the representative signal contribution for a monopole of mass 100 GeV, and the arrow in the ratio plot is for the point that is outside the range.

Figure 4 (right) shows the T variable distribution in the CR1, the VR and the SR. With the good agreement between the background template and the data, one can estimate the background contribution in the signal region to be 4 ± 4 events.

3.3 XnXn correction

For a proper description of the data by the signal Monte Carlo, an extra correction considering the different event topologies needs to be applied. The correction factor is derived in the form of the effective probability of having an event with $XnXn$ topology:

$$p^{eff}_{XnXn} = 0.8 \cdot (2 \cdot f_{0nXn} \cdot p_{EMPU} + f_{XnXn}) \cdot (1 + f_{diss}), \tag{3}$$

where f_{0nXn} and f_{XnXn} are predicted fractions of events with single and double EM breakup respectively, p_{EMPU} is the probability of electromagnetic pile-up, and f_{diss} is the small fraction of dissociative dilepton events. The f_{0nXn} and f_{XnXn} are obtained from SuperChic Monte Carlo generator predictions [19], p_{EMPU} is estimated to be 0.038 for signal trigger and 2023 Pb+Pb data-taking conditions, and $f_{diss} = 0.13$ based on the study of exclusive dimuon and dielectron events [2,3]. An extra 0.8 factor accounts for mismodelling of f_{0nXn} and f_{XnXn} in SuperChic. The model is then validated on the UPC $\gamma\gamma \to \mu^+\mu^-$ events in three rapidity bins, shown in Figure 5. A good agreement between model and the data is found.

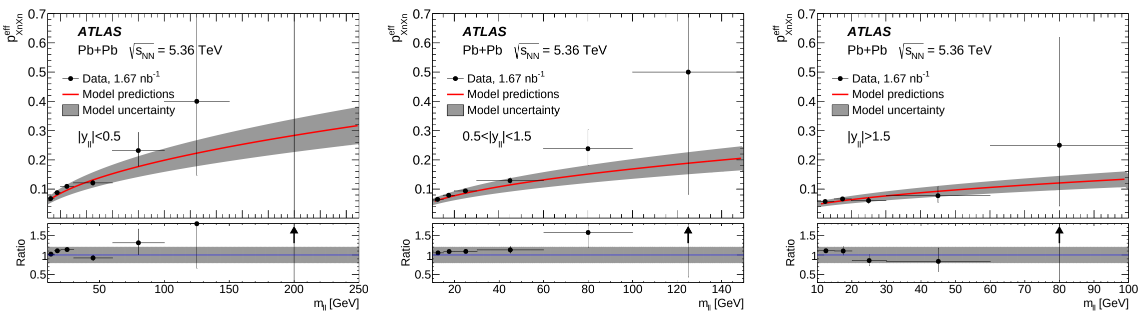

Figure 5 – The values of p^{eff}_{XnXn} extracted from data as a function of dilepton invariant mass for several dilepton rapidity regions: (left) —y_{ll}— ¡ 0.5, (middle) 0.5 ¡ —y_{ll}— ¡ 1.5 and (right) —y_{ll}— ¿ 1.5. The results are compared with predictions based on SuperChic 4.2. The shaded band denotes model uncertainty on p^{eff}_{XnXn}. The bottom panels show data-to-model ratios. The arrows in the ratio plots are for the points that are outside the range.

4 Systematic uncertainties

The systematic uncertainties considered are related to the modelling of the detector response to the monopole, the overall noise level in the pixel detector and calorimeters, potential mismodelling of the $XnXn$ selection, the background uncertainty, and the luminosity uncertainty. The largest uncertainties are attributed to the $XnXn$ selection modelling (20%) and the detector material modelling (up 20% for highest masses), with the remaining sources ranging between less-than-one to a few percent. The total systematic uncertainty varies between 21% (lowest) and 38% (highest masses).

5 Magnetic monopole production limits

Three events were found in the SR, which is consistent with the background estimate of 4 ± 4 events. The exclusion limits are set at 95% confidence level (CL) using the CL_s method [20] and are shown in Figure 6. The limits are calculated using the pseudo-experiment approach, with 20,000 pseudo-experiments per mass point. The FPA model predictions [9], with the alternative predictions from the LCFA model [9,10,11,12], and the limits observed by MoEDAL [11] are compared to the ATLAS results [6]. The presented search significantly improves on the results from the previous cross-section limits reported by MoEDAL for $|q_m| = 1g_D$ and allows excluding magnetic monopoles with masses below 120 GeV, assuming the FPA model. By assuming the LCFA model, the magnetic monopoles with masses below 80 GeV are excluded.

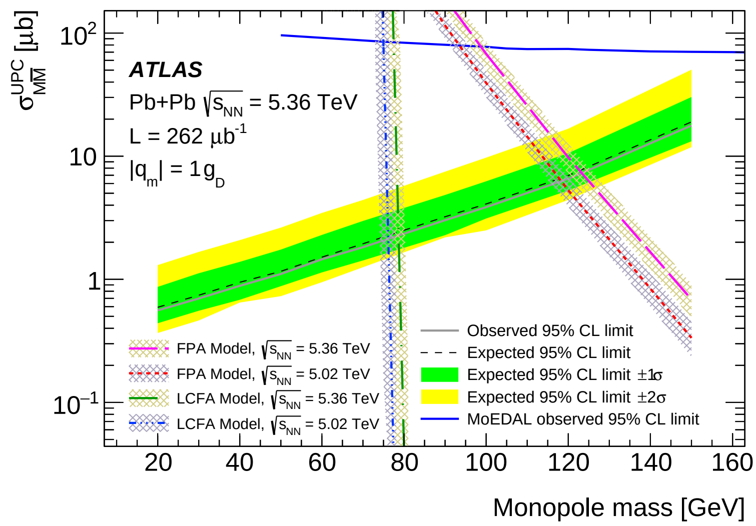

Figure 6 – Expected and observed upper limits on the monopole pair-production cross-section in Pb+Pb UPC at $\sqrt{s_{\rm NN}} = 5.36$ TeV for $|q_m| = 1$gD and assuming the FPA model. The gray solid line (black dashed line) represents observed (expected) limits, whereas the darker and lighter shaded bands around the expected limits represent the $\pm 1\sigma$ and $\pm 2\sigma$ intervals, respectively. The FPA [9] (magenta and red lines) and LCFA [9,10,11,12] (green and blue lines) models predictions and the observed limits by MoEDAL [11] for $|q_m| = 1$gD at a lower centre-of-mass energy of $\sqrt{s_{\rm NN}} = 5.02$ TeV (blue line) are compared to limits obtained by ATLAS [6]. The two sets of model curves (5.36 TeV and 5.02 TeV) are shown to allow a comparison of the theoretical predictions at different centre-of-mass energies, relevant for ATLAS and MoEDAL experiments, respectively.

6 Summary

A summary of the search for magnetic monopole production with mass range between 20 GeV and 150 GeV in ultraperipheral collisions using 262 μb^{-1} of Pb+Pb data at $\sqrt{s_{\rm NN}} = 5.36$ TeV, collected by the ATLAS experiment in 2023 is presented. This search uses a novel method of detecting low-mass magnetic monopoles in UPC collisions which is complementary to the one used by the MoEDAL experiment. The derived upper limits on monopole pair-production cross-sections are more stringent than the limits reported by MoEDAL. Magnetic monopoles with magnetic charge equal to one Dirac charge and masses below 120 GeV are excluded, assuming the FPA model. This new approach can be further explored for other similar searches.

Acknowledgments

Research project partly supported by program "Excellence initiative – research university" for the AGH University of Kraków, project no. 9722.

References

1. Lyndon Evans and Philip Bryant. LHC Machine. *JINST*, 3:S08001, 2008.
2. ATLAS Collaboration. Exclusive dimuon production in ultraperipheral Pb+Pb collisions at $\sqrt{s_{\text{NN}}} = 5.02\,\text{TeV}$ with ATLAS. *Phys. Rev. C*, 104:024906, 2021.
3. ATLAS Collaboration. Exclusive dielectron production in ultraperipheral Pb+Pb collisions at $\sqrt{s_{\text{NN}}} = 5.02\,\text{TeV}$ with ATLAS. *JHEP*, 06:182, 2023.
4. ATLAS Collaboration. Observation of the $\gamma\gamma \to \tau\tau$ Process in Pb+Pb Collisions and Constraints on the τ-Lepton Anomalous Magnetic Moment with the ATLAS Detector. *Phys. Rev. Lett.*, 131:151802, 2023.
5. ATLAS Collaboration. Measurement of light-by-light scattering and search for axion-like particles with 2.2 nb^{-1} of Pb+Pb data with the ATLAS detector. *JHEP*, 03:243, 2021.
6. ATLAS Collaboration. Search for Magnetic Monopole Pair Production in Ultraperipheral Pb+Pb Collisions at $\sqrt{s_{\text{NN}}} = 5.36\,\text{TeV}$ with the ATLAS Detector at the LHC. *Phys. Rev. Lett.*, 134:061803, 2025.
7. Paul Adrien Maurice Dirac. Quantised singularities in the electromagnetic field,. *Proc. Roy. Soc. Lond. A*, 133(821):60–72, 1931.
8. Julian Schwinger. On gauge invariance and vacuum polarization. *Phys. Rev.*, 82:664–679, 1951.
9. Oliver Gould, D. L.-J. Ho, and Arttu Rajantie. Towards Schwinger production of magnetic monopoles in heavy-ion collisions. *Phys. Rev. D*, 100(1):015041, 2019.
10. Oliver Gould, D. L.-J. Ho, and Arttu Rajantie. Schwinger pair production of magnetic monopoles: Momentum distribution for heavy-ion collisions. *Phys. Rev. D*, 104(1):015033, 2021.
11. MoEDAL Collaboration. Search for magnetic monopoles produced via the Schwinger mechanism. *Nature*, 602(7895):63–67, 2022.
12. MoEDAL Collaboration. MoEDAL Search in the CMS Beam Pipe for Magnetic Monopoles Produced via the Schwinger Effect. *Phys. Rev. Lett.*, 133(7):071803, 2024.
13. ATLAS Collaboration. The ATLAS Experiment at the CERN Large Hadron Collider. *JINST*, 3:S08003, 2008.
14. ATLAS Collaboration. The ATLAS experiment at the CERN Large Hadron Collider: a description of the detector configuration for Run 3. *JINST*, 19:P05063, 2024.
15. ATLAS Collaboration. The ATLAS trigger system for LHC Run 3 and trigger performance in 2022. *JINST*, 19:P06029, 2024.
16. ATLAS Collaboration. Software and computing for Run 3 of the ATLAS experiment at the LHC. *Eur. Phys. J. C*, 85:234, 2025.
17. ATLAS Collaboration. Characterisation and mitigation of beam-induced backgrounds observed in the ATLAS detector during the 2011 proton–proton run. *JINST*, 8:P07004, 2013.
18. ATLAS Collaboration. Measurement of distributions sensitive to the underlying event in inclusive Z boson production in pp collisions at $\sqrt{s} = 13\,\text{TeV}$ with the ATLAS detector. *Eur. Phys. J. C*, 79:666, 2019.
19. L. A. Harland-Lang. Exciting ions: A systematic treatment of ultraperipheral heavy ion collisions with nuclear breakup. *Phys. Rev. D*, 107:093004, May 2023.
20. Alexander L. Read. Presentation of search results: the CL_s technique. *J. Phys. G*, 28:2693, 2002.